Short Communication:

Environmentally Friendly and Facile Solid-State Synthesis of Nanostructured Cobalt Ferrites

Khoa Dang Nguyen[1,2], Khoa Dang Tran[1,2], Van Thi Tuong Pham[1,2*], and Ha Vu Le[1,2]**

[1]*Faculty of Chemical Engineering, Ho Chi Minh City University of Technology (HCMUT), 268 Ly Thuong Kiet Street, District 10, Ho Chi Minh City 740010, Vietnam*

[2]*Vietnam National University Ho Chi Minh City, Linh Trung Ward, Thu Duc District, Ho Chi Minh City 720325, Vietnam*

** **Corresponding author:***

tel: +84-838647256
email: pttvan.sdh231@hcmut.edu.vn; lvha@hcmut.edu.vn***

Received: August 14, 2024
Accepted: September 19, 2024

DOI: 10.22146/ijc.99143

Abstract: *In this study, a simple and solvent-free grinding method was employed to produce nanostructured cobalt ferrites ($CoFe_2O_4$). Their morphology and textural properties were notably found to be impacted by the calcination. Notably, the prepared material calcinated at 250 °C exhibited high mesoporosity with a surface area of 186 m^2 g^{-1} and a pore size of approximately 3.2 nm, while the highly crystalline $CoFe_2O_4$ with sparse pore structure would tend to be more favorable as increasing calcination temperatures. At 550 °C, the $CoFe_2O_4$ material specifically formed a well-defined shape, albeit with non-uniform particle sizes ranging from 40 to 80 nm. These distinct nanostructures were completely lost upon calcination at 900 °C, resulting in a bulk $CoFe_2O_4$ with a very high crystallinity. Furthermore, the study also investigated the influence of polyvinylpyrrolidone (PVP) on the structure and morphology of as-prepared $CoFe_2O_4$. It was observed that PVP could mitigate sintering, leading to the increase in the surface area of $CoFe_2O_4$ calcined at 550 °C due to the decrease in nanoparticle size.*

Keywords: *cobalt ferrites; mechanochemistry; nanostructure; polyvinylpyrrolidone*

■ INTRODUCTION

Nanostructure spinel ferrites have attracted much interest in recent years due to their outstanding magnetic behavior, viable surface modification, and broad applications in many industrial fields, including environmental treatment, catalysis, and biomedical and electronic techniques [1-5]. Among spinel ferrites, cobalt ferrite ($CoFe_2O_4$) is a common magnetic oxide with an inverse spinel structure, which has a high intrinsic coercivity, moderate saturation magnetization, and great physical and chemical stability. These properties are essential to improve recording, hyperthermia, targeted drug delivery, and resonance imaging [6]. Importantly, it has been demonstrated that the magnetic characteristics of $CoFe_2O_4$ can be influenced by particle size, morphology, and structure, which can be adjusted via synthetic parameters. Therefore, various fabrication methods for $CoFe_2O_4$ have been investigated to obtain desired physical and chemical properties, including sol-gel auto combustion, hydrothermal combustion, microemulsion, co-precipitation, microwave-assisted synthesis, polyol-involving route, and aerosol method [7-9]. Although most of these techniques can produce $CoFe_2O_4$ with well-defined sizes and shapes, they are often hampered by significant drawbacks such as high cost, complexity, extensive use of solvents and additives, and prolonged reaction times [10].

The solid-state approach has been widely applied to synthesize nanomaterials due to its ability to circumvent the use of hazardous organic solvents. This technique is valued for its simplicity, speed, scalability, cost-effectiveness, and environmental friendliness, leading to increased attention in the field of chemistry [11]. For instance, bismuth-doped halide perovskites were successfully synthesized with high crystallinity and excellent microstructure through solvent-free grinding of methylammonium iodide and metal precursors in

various ratios, offering a promising alternative to lead-containing perovskite solar cells [12]. Furthermore, mixing metal precursor salts and sodium hydroxide as a hydrolysis reagent, followed by calcination at high temperatures, produced copper ferrite ($CuFe_2O_4$) with particle size of nanoparticles ranging from 75 to 116 nm [13]. Akbari Moayyer and Ataie [14] prepared $CoFe_2O_4$ nanoparticles using a ceramic manner involving a mixture of cobalt carbonate and iron oxide, resulting in $CoFe_2O_4$ with a mean crystallite of 49 nm and particle size of 300 nm after calcination at 1000 °C, exhibiting hard magnetic properties [14]. In this study, nanostructured $CoFe_2O_4$ were facilely synthesized via the grinding method without needing any solvent for the reaction. The structural and morphological characteristics of as-synthesized $CoFe_2O_4$ samples were thoroughly examined using X-ray diffraction, transmission electron microscopy, thermogravimetry analysis, and isothermal nitrogen sorption measurements. Moreover, the influence of using polyvinylpyrrolidone (PVP) on the particle size and distribution of the resulting $CoFe_2O_4$ was investigated.

■ EXPERIMENTAL SECTION

Materials

All chemicals and starting materials were purchased from Sigma-Aldrich and used as received without any purification. Cobalt(II) nitrate hexahydrate ($Co(NO_3)_2{\cdot}6H_2O$, purity 98%), iron(III) nitrate nonahydrate ($Fe(NO_3)_3{\cdot}9H_2O$, purity 98%), sodium hydroxide (NaOH, purity 97%), sodium chloride (NaCl, purity 96%), and cross-linked PVP (M = 3500 g mol^{-1}) were used as precursors.

Instrumentation

Thermogravimetric analysis (TGA) was conducted on the TA Instruments SDT Q600 Thermal Gravimetric Analyzer. Approximately 10 mg of sample was loaded into an alumina pan for each measurement, which was then heated from 30–800 °C at a rate of 5 °C min^{-1} in the air atmosphere. Nitrogen adsorption isotherm measurements were performed at 77 K on a Micromeritics Tristar device after the sample was treated at 120 °C under reduced pressures for 10 h. The specific surface area was calculated in a relative pressure range of p/p_0 = 0.05–0.30 using the Brunauer–Emmett–Teller (BET) model. X-ray diffraction (XRD) measurements were performed on a D8 Advance Bruker Diffractometer using CuK_α radiation in a 2θ range of 10–80° (0.0105° step^{-1} and 0.63° min^{-1}). TEM was recorded on an EM1010–Jeol electron microscope.

Procedure

Synthesis of $CoFe_2O_4$

$CoFe_2O_4$ was prepared via a grinding method based on the reported study of Zeynizadeh et al. [13] on the synthesis of $CuFe_2O_4$ magnetically nanoparticles, with modifications. Initially, 1.455 g (0.005 mol) of $Co(NO_3)_2{\cdot}6H_2O$, 4.040 g (0.010 mol) of $Fe(NO_3)_3{\cdot}9H_2O$, and 1.167 g (0.020 mol) of NaCl was grounded in a porcelain mortar for 10 min. Subsequently, the mixture was added with 1.600 g (0.04 mol) of NaOH and was ground for a further 50 min before being washed with water several times until neutralization was achieved. After centrifugation, the collected solid was dried at 80 °C overnight and subsequently treated in the air at different temperatures, including 250, 350, 450, 550, and 900 °C for 4 h with a rate of 2 °C min^{-1}, resulting in a black powder denoted as $CoFe_2O_4$-T, where T represents the corresponding calcination temperature applied.

Synthesis of $CoFe_2O_4$ in the presence of PVP

$CoFe_2O_4$-PVP was synthesized by following the procedure described above in the presence of PVP. In a porcelain mortar, a mixture of 2.0 g of PVP, 1.455 g (0.005 mol) of $Co(NO_3)_2{\cdot}6H_2O$, 4.040 g (0.010 mol) of $Fe(NO_3)_3{\cdot}9H_2O$, and 1.169 g (0.020 mol) of NaCl was grounded in 10 min. An amount of 1.600 g (0.040 mol) of NaOH was then added to the mixture and ground for 50 min. Subsequently, it was rinsed with distilled water and dried at 80 °C for 12 h. The resulting powder was calcined at 550 °C for 4 h (2 °C min^{-1}) to generate the final product denoted as $CoFe_2O_4$-PVP-550.

■ RESULTS AND DISCUSSION

In a typical experiment, a mixture of $Co(NO_3)_2{\cdot}6H_2O$, $Fe(NO_3)_3{\cdot}9H_2O$, and NaCl (as shown in Fig. 1(a)) was intensively ground for 10 min in a

porcelain mortar. Among various metal salts, nitrate salts are preferred to other metal salts in the synthesis of metal oxides due to their good solubility in water and low decomposition temperatures, leading to few residual contaminants in the final products [15-17]. Meanwhile, the NaCl salt was used as a capping agent to prevent particle agglomeration and control their growth [18]. Afterward, a stoichiometric amount of NaOH was added to the mixture, and grinding continued for another 50 min. During this process, the color of the mixtures gradually changed from red-orange (Fig. 1(b)) to black (Fig. 1(c)), indicating the occurrence of basic hydrolysis of the cobalt and ferric salts, leading to the formation of the black $CoFe_2O_4$ phase (Eq. 1).

$$2Fe(NO_3)_3+Co(NO_3)_2+8NaOH \rightarrow CoFe_2O_4+4H_2O+8NaNO_3 \quad (1)$$

The sodium salts were then removed by simple washing with excess distilled water. The collected solid was dried at 80 °C to remove free water and subsequently calcined at an elevated temperature (250–900 °C) to dehydrate surface metal hydroxides, resulting in the formation of crystalline $CoFe_2O_4$.

TGA was performed to investigate the thermal behavior of the $CoFe_2O_4$ sample dried at 80 °C, focusing on weight (%) as a function of temperature (Fig. 2). Two main stages of weight loss were observed in the temperature range from 30 to 800 °C. The initial weight loss of 6% occurred at the temperature region below 100 °C, attributed to the removal of physically adsorbed water in the $CoFe_2O_4$ sample. The subsequent weight loss stage, observed from 100 to approximately 250 °C,

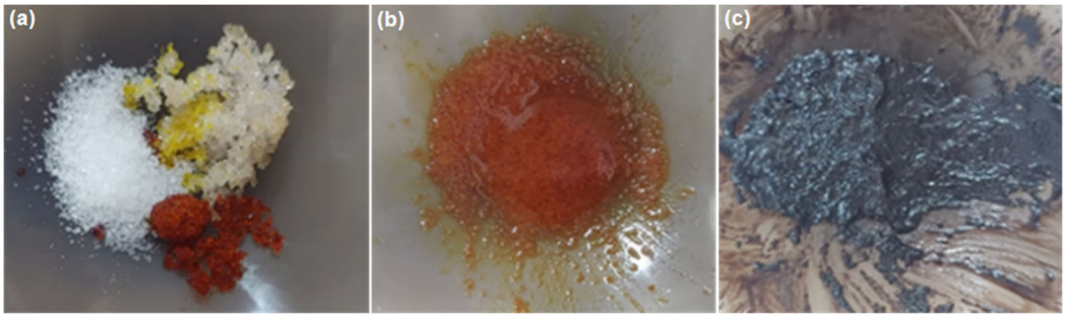

Fig 1. Photographs of the initial mixture of $Fe(NO_3)_3{\cdot}9H_2O$, $Co(NO_3)_2{\cdot}6H_2O$, and NaCl (a) before grinding, (b) after 10 min of grinding the mixture, (c) after adding NaOH to the mixture and grinding for a further 50 min

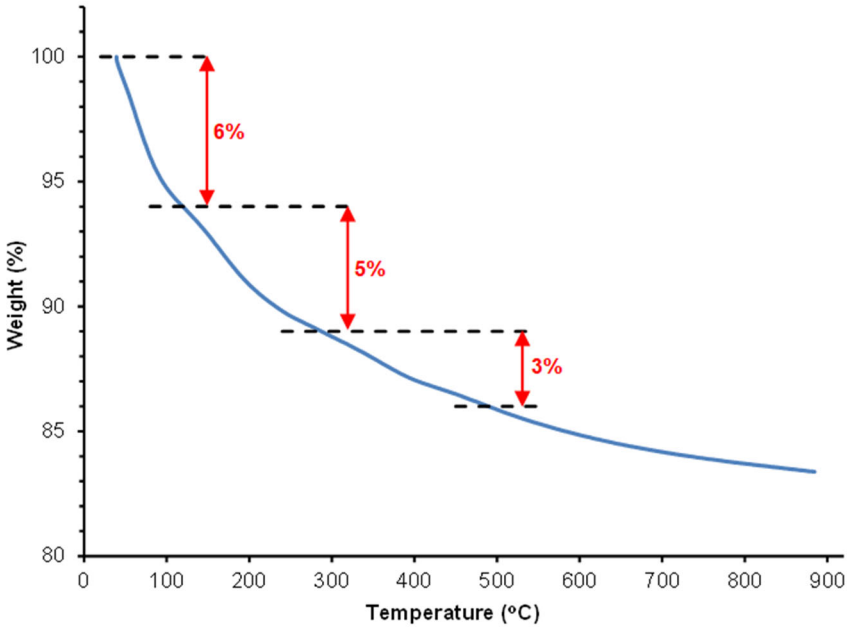

Fig 2. TGA curve for $CoFe_2O_4$ sample after drying at 80 °C

was due to the removal of coordinated water adsorbed at the surface of $CoFe_2O_4$ and the dehydration of the metal hydroxides. These findings aligned with previous studies on the preparation of $CoFe_2O_4$ using co-precipitation or solvothermal methods [19-20]. Further treatment of the sample at higher temperatures resulted in a negligible weight decrease, indicating the completion of hydration and the formation of the $CoFe_2O_4$ phase. Therefore, the calcination step for the preparation of nanostructured $CoFe_2O_4$ was performed at various temperatures above 250 °C, allowing for changes in the structure and morphology of $CoFe_2O_4$ to be observed.

Fig. 3 shows the XRD patterns of $CoFe_2O_4$ calcined from 250 to 900 °C. The peaks were observed at 2θ = 18.5°, 30.1°, 35.2°, 37.1°, 43.0°, 53.4°, 56.9°, and 62.6°, corresponding to (111), (220), (311), (222), (400), (422), (511) and (440) crystallographic planes of the spinel structure of ferrites, indicating the formation of crystalline $CoFe_2O_4$ [19,21]. Upon annealing at 250 °C for 4 h in air, the XRD result revealed broad and low-intensity characteristic peaks of $CoFe_2O_4$, suggesting a small particle size and low crystallinity. Notably, the diffraction peak intensity increased significantly with the calcination temperature due to the growth of the $CoFe_2O_4$ crystals, likely resulting from particle sintering at high temperatures. However, an extra peak at 2θ = 33.29° observed in the XRD patterns of samples calcined at 500 and 900 °C was assigned to the (104) plane of the hematite (α-Fe_2O_3), possibly due to heterogeneous reaction conditions and higher reactivity of the Fe^{3+} species [22]. The presence of this hematite phase has also been reported in previous studies on $CoFe_2O_4$ [23-24].

Next, the morphology of $CoFe_2O_4$ calcined at different temperatures was examined in the TEM images (Fig. 4). As expected, increasing the calcination temperature caused significant changes in the morphology and size of $CoFe_2O_4$ particles. Small nanoparticles (20–30 nm) were observed for the sample treated at 250 °C; however, the separation of these nanoparticles was unclear. Meanwhile, well-defined and larger nanoparticles ranging from 20 to 80 nm were formed when $CoFe_2O_4$ was annealed at higher temperatures (350–550 °C). The irregular morphology of the nanoparticles was attributed to the solid-state reaction via grinding. These observations were indeed in good agreement with the XRD results described above. Notably, the particle agglomeration was complete at 900 °C, leading to the formation of the bulk $CoFe_2O_4$ phase.

In general, the nitrogen physisorption isotherms of the samples showed a large quantity adsorbed at relative pressures of 0.40 to 0.99, which are typical for mesoporous and macroporous structures (Fig. 5(a)) [25].

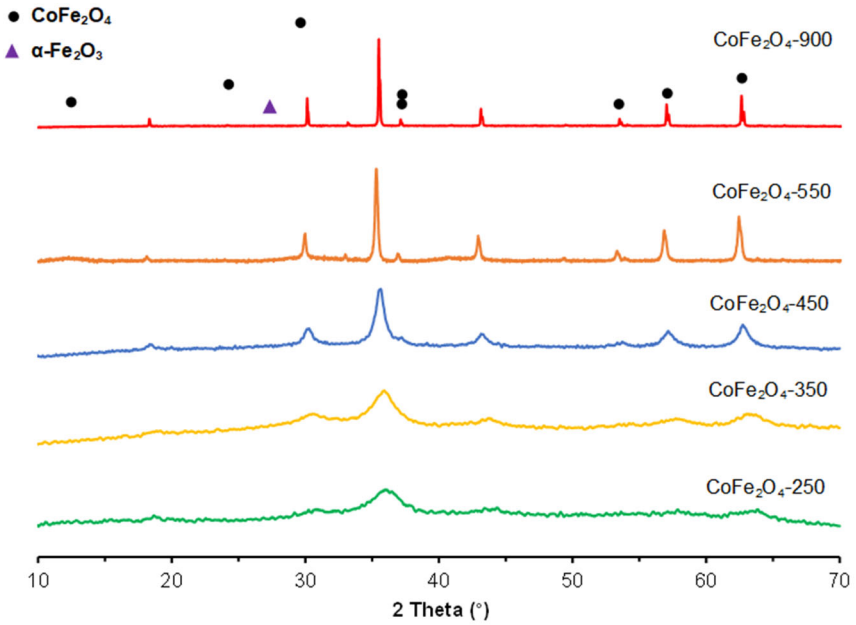

Fig 3. XRD results of $CoFe_2O_4$ samples calcined at varied temperatures

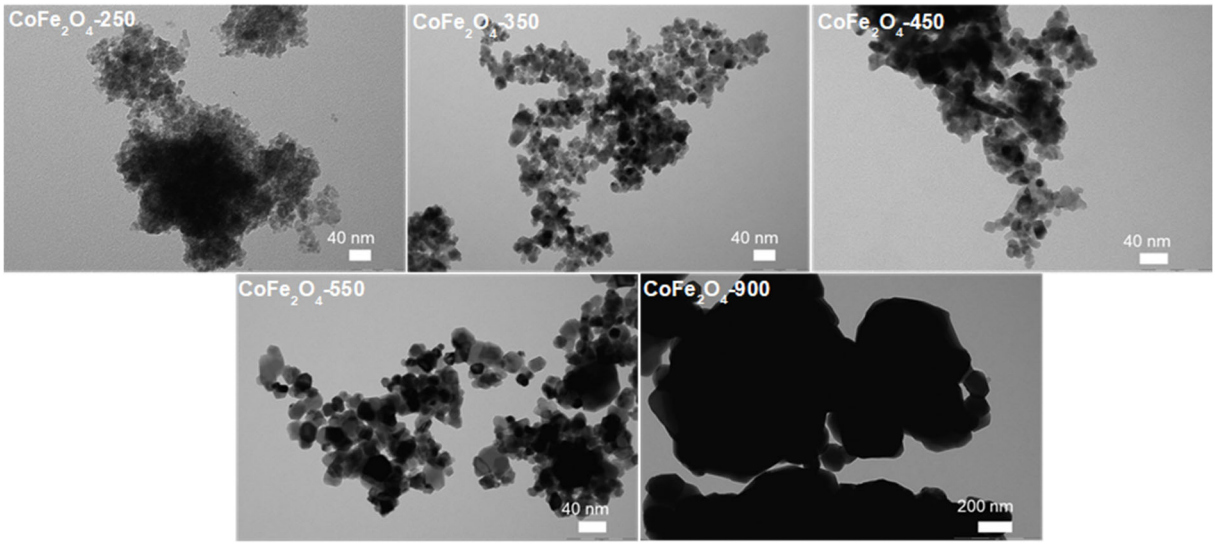

Fig 4. TEM images of $CoFe_2O_4$ samples prepared at different calcination temperatures

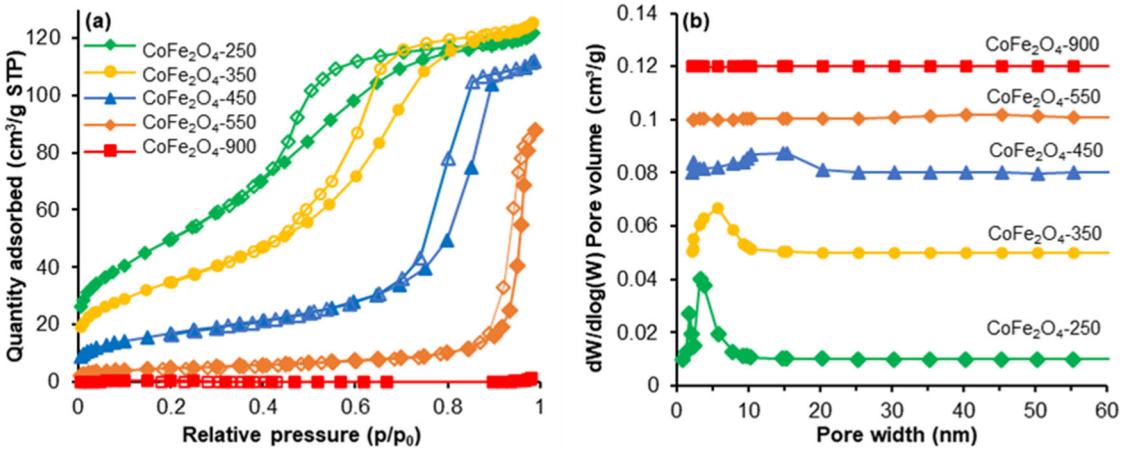

Fig 5. (a) Nitrogen sorption isotherms and (b) pore size distribution calculated by DFT method of $CoFe_2O_4$ samples, calcined at different temperatures

As expected, the BET surface area of $CoFe_2O_4$-250 was the highest among the samples, with a value of 186 $m^2 g^{-1}$ (Entry 1, Table 1), indicating the formation of capillaries in the structure. The average pore size for this sample was determined to be approx. 3.5 nm, falling within the mesoporous region, which contributed to most of the total pore volume and surface area. These mesopores could be attributed to the free spaces between the nanoparticle clusters, as observed in the TEM images (Fig. 5(b)). Moreover, it is evident that the surface area rapidly decreases with the increase in the calcination temperature due to the enhanced isolation and agglomeration of the particles. Indeed, treatment of $CoFe_2O_4$ at 350, 450, and 550 °C resulted in surface areas of 128, 60, and 17 $m^2 g^{-1}$, respectively, while a negligible surface area was obtained for the samples annealed at 900 °C due to the formation of bulk material (Entries 2-5, Table 1). In these cases, the obtained surface areas of $CoFe_2O_4$ could be related to the

Table 1. BET surface areas of the $CoFe_2O_4$ samples calcined at varied temperatures

Entry	Sample	S_{BET} ($m^2 g^{-1}$)
1	$CoFe_2O_4$-250	186.0
2	$CoFe_2O_4$-350	128.0
3	$CoFe_2O_4$-450	60.0
4	$CoFe_2O_4$-550	17.0
5	$CoFe_2O_4$-900	0.6

overall particle surface. It should be noted that the surface areas of the as-prepared $CoFe_2O_4$ samples are generally higher than those reported in the previous studies in which the grinding method was also used [26].

PVP was employed as a surface capping agent in the synthesis of $CoFe_2O_4$ to prevent particle aggregation and control the particle size and shape through the interactions between PVP and metal ions. Co^{2+} and Fe^{3+} ions are believed to adhere to the polymer surface via electrostatic interactions between the metal cations and the amide group in the polymeric chain, resulting in a good dispersion of the metal hydroxide species in the cavities and network of PVP. Nanoparticles with high surface energy tend to sinter and grow larger during the calcination stage via the Ostwald ripening process [27]. Therefore, PVP played an important role in sterically hindering the agglomeration of the nanoparticles during this stage. As mentioned in the literature, steric hindrance likely arises from bulky substances and repulsive forces between the polymeric functional groups [8]. In the PVP-involved procedure, PVP was subsequently removed after the rinsing process due to its hydrophilicity. However, this washing might have been incomplete, allowing PVP to remain in the solid phase during calcination and beneficially preventing nanoparticle agglomeration at high temperatures.

The presence of unwashed PVP can be confirmed by the TGA analysis, as shown in Fig. 6 and Table 2, compared with that of the PVP-free sample. Similar to the PVP-free samples, $CoFe_2O_4$ synthesized with PVP showed two typical drops of weight in the temperature ranges of 50–100 °C and 100–250 °C, attributed to the removal of free and adsorbed water molecules as well as dehydration of the surface hydroxide phases. However, a significant difference was observed between the samples with and without PVP, in which a major weight loss of 27% assigned to decomposition and burning of the PVP polymer chains in the presence of oxygen emerged,

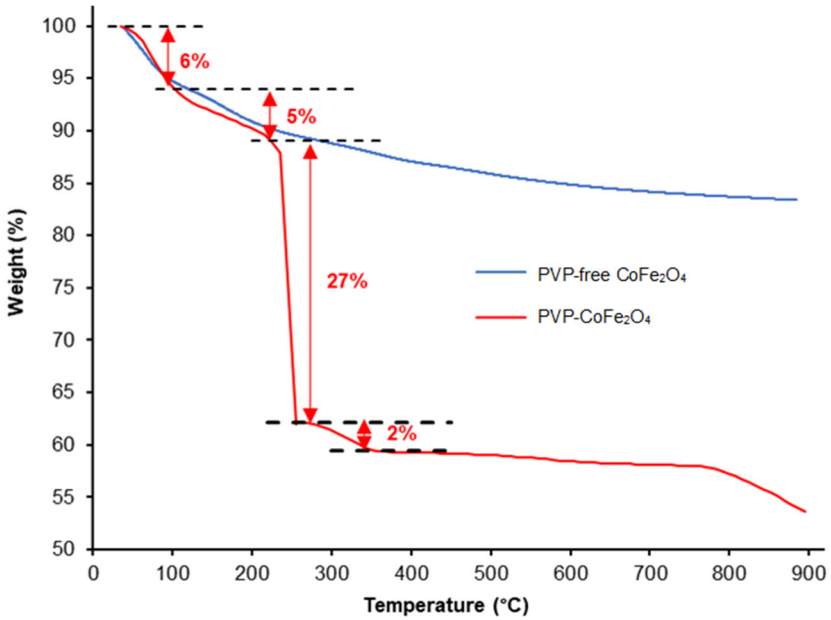

Fig 6. The TGA curves of the $CoFe_2O_4$ samples were synthesized with PVP and without PVP after drying at 80 °C

Table 2. Summary of TGA results of $CoFe_2O_4$-550 and $CoFe_2O_4$-PVP-550 samples

Sample	1st stage		2nd stage		3rd stage		4th stage	
	Temp. range (°C)	ΔW_1 (wt.%)	Temp. range (°C)	ΔW_2 (wt.%)	Temp. range (°C)	ΔW_3 (wt.%)	Temp. range (°C)	ΔW_4 (wt.%)
PVP-free $CoFe_2O_4$	30–100	6	100–250	5	250–500	3	-	-
PVP $CoFe_2O_4$	30–100	6	100–250	5	250–270	27	270–400	2

indicating a considerable amount of PVP remained in $CoFe_2O_4$ after washing with water [28]. These remaining PVP species could evidently reduce the agglomeration of particles at high temperatures and improve the nanostructure of cobalt ferrite. Above 400 °C, no significant weight loss was observed, indicating the complete removal of PVP from the $CoFe_2O_4$ phase. Subsequent characterizations will focus on samples calcined at 550 °C under the PVP-free conditions and in the presence of PVP.

PXRD patterns of $CoFe_2O_4$-PVP-550 confirmed the formation of the crystalline $CoFe_2O_4$ phase similar to that of $CoFe_2O_4$-550 (Fig. 7) [29]. However, the diffraction peaks of $CoFe_2O_4$-PVP were broader and less sharp compared to those of $CoFe_2O_4$-550, indicating a reduction in the crystallinity and particle size as a result of using PVP as a dispersive agent in the $CoFe_2O_4$ framework, hindering the particle growth during the calcination process [30]. Furthermore, the morphology of the $CoFe_2O_4$ sample calcined at 550 °C was compared via the TEM analysis shown in Fig. 8. The application of PVP in the preparation of $CoFe_2O_4$ allowed the formation of nanoparticles in smaller and more uniform sizes ranging from 15 to 30 nm compared to that of the sample prepared without PVP. Significantly, the BET surface area of $CoFe_2O_4$ increased from 17 to 40 $m^2 g^{-1}$ with the addition of PVP to the precursor mixture (Fig. 9). These characterization results indeed demonstrated that PVP could significantly improve the synthesis of $CoFe_2O_4$ nanoparticles.

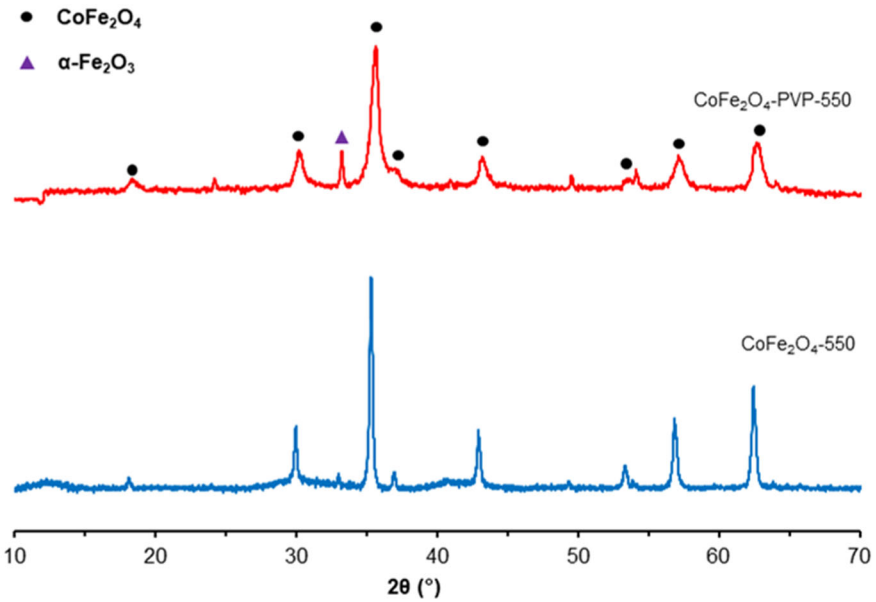

Fig 7. XRD patterns of $CoFe_2O_4$-550 and $CoFe_2O_4$-PVP-550 samples

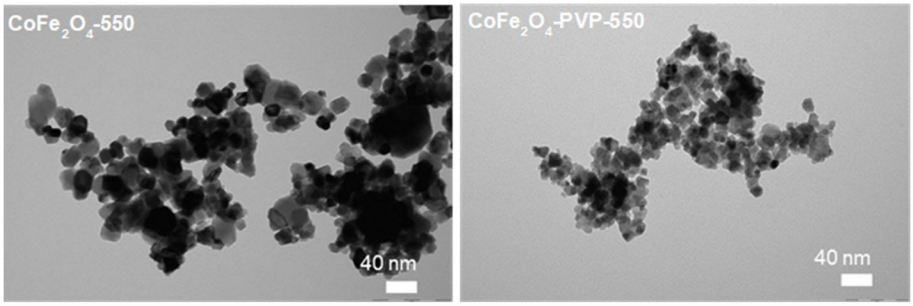

Fig 8. TEM images of $CoFe_2O_4$-550 and $CoFe_2O_4$-PVP-550 samples

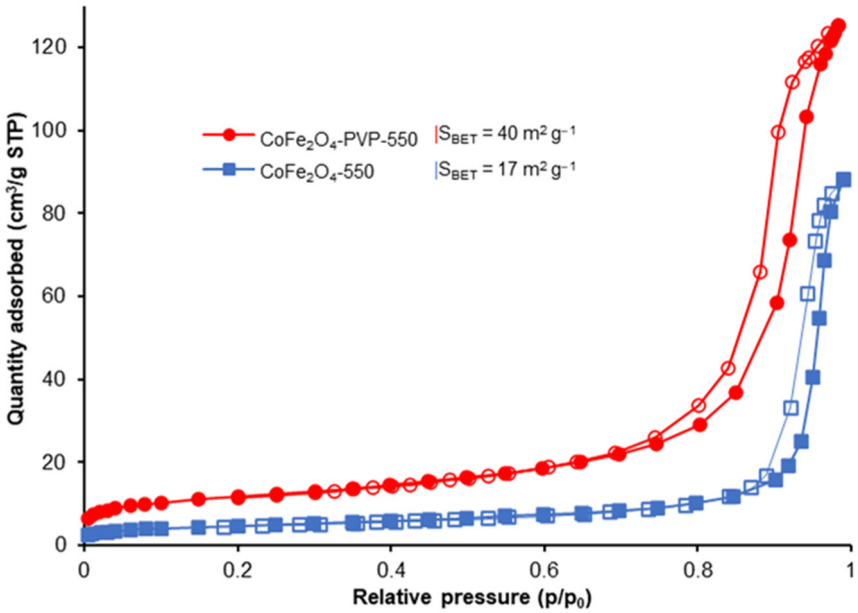

Fig 9. Nitrogen sorption isotherms and BET surface areas of $CoFe_2O_4$-550 and $CoFe_2O_4$-PVP-550 samples

■ CONCLUSION

In summary, nanostructured $CoFe_2O_4$ were fabricated from readily available reagents under grinding conditions. The characterization results demonstrated the effect of calcination temperature on the particle size and morphology of the samples. A mesoporous structure with a surface area of 186 $m^2 g^{-1}$ was obtained at a low calcination temperature (250 °C). The synthesized particle size was from 20 to 80 nm as the samples were annealed below 550 °C while bulk $CoFe_2O_4$ was formed due to the agglomeration of particles at 900 °C. In addition, the influence of using PVP in the ground precursor mixture on the crystallinity, morphology, and particle size of the resulting $CoFe_2O_4$ sample was investigated. The TEM analysis displayed that the nanoparticle size of $CoFe_2O_4$ could be controlled by the presence of PVP, which prevented interparticle interaction and thus reduced agglomeration. This study offers an efficient, simple, and environmentally friendly route for the fabrication of $CoFe_2O_4$ nanoparticles, with the potential for large-scale production.

■ ACKNOWLEDGMENTS

We acknowledge Ho Chi Minh City University of Technology (HCMUT) VNU-HCM for supporting this study. We also would like to thank Vy T.B. Nguyen for supporting the experiments.

■ CONFLICT OF INTEREST

The authors declare that they have no known competing financial interests or personal relationships that could have appeared to influence the work reported in this paper.

■ AUTHOR CONTRIBUTIONS

Conceptualization and supervision, Khoa Dang Nguyen, Ha Vu Le; Data curation, Khoa Dang Nguyen, Ha Vu Le, Van Thi Tuong Pham, Khoa Dang Tran; Methodology, Van Thi Tuong Pham, Ha Vu Le; Analysis, Khoa Dang Nguyen, Ha Vu Le, and Van Thi Tuong Pham; Writing-original draft, Van Thi Tuong Pham, Khoa Dang Tran, Writing-review and editing, Van Thi Tuong Pham, Khoa Dang Tran, Ha Vu Le. All authors have read and agreed to the published version of the manuscript.

■ REFERENCES

[1] Kunarti, E.S., Agustiningsih, D., Pambudi, F.I., Syoufian, A., and Santosa, S.J., 2025, Enhanced photocatalytic activity and magnetic properties of $CoFe_2O_4/TiO_2$-Ag/S for visible light-driven

photodegradation of methylene blue, *Indones. J. Chem.*, 25 (1), 232–243.

[2] Amiri, M., Pardakhti, A., Ahmadi-Zeidabadi, M., Akbari, A., and Salavati-Niasari, M., 2018, Magnetic nickel ferrite nanoparticles: Green synthesis by *Urtica* and therapeutic effect of frequency magnetic field on creating cytotoxic response in neural cell lines, *Colloids Surf., B*, 172, 244–253.

[3] Karthickraja, D., Karthi, S., Kumar, G.A., Sardar, D.K., Dannangoda, G.C., Martirosyan, K.S., and Girija, E.K., 2019, Fabrication of core–shell $CoFe_2O_4$@HAp nanoparticles: A novel magnetic platform for biomedical applications, *New J. Chem.*, 43 (34), 13584–13593.

[4] Perumbilavil, S., López-Ortega, A., Tiwari, G.K., Nogués, J., Endo, T., and Philip, R., 2018, Enhanced ultrafast nonlinear optical response in ferrite core/shell nanostructures with excellent optical limiting performance, *Small*, 14 (6), 1701001.

[5] Nguyen, K.D., Tran, K.D., Le, H.V., Pham, V.T.T., and Ho, P.H., 2024, Enhanced Fenton-photocatalytic degradation of rhodamine B over cobalt ferrite nanoparticles synthesized by a polyvinylpyrrolidone-assisted grinding method, *Inorg. Chem.*, 63 (50), 23586–23600.

[6] Kim, D.H., Nikles, D.E., Johnson, D.T., and Brazel, C.S., 2008, Heat generation of aqueously dispersed $CoFe_2O_4$ nanoparticles as heating agents for magnetically activated drug delivery and hyperthermia, *J. Magn. Magn. Mater.*, 320 (19), 2390–2396.

[7] Fariñas, J.C., Moreno, R., Pérez, A., García, M., García-Hernández, M., Salvador, M., and Borrell, A., 2018, Microwave-assisted solution synthesis, microwave sintering and magnetic properties of cobalt ferrite, *J. Eur. Ceram. Soc.*, 38 (5), 2360–2368.

[8] Wei, Y., and Liu, Y., 2019, Study of dispersion mechanisms of modified SiC powder: Electrostatic repulsion and steric hindrance mechanism, *New J. Chem.*, 43 (35), 14036–14044.

[9] Venturini, J., Piva, D.H., da Cunha, J.B.M., and Bergmann, C.P., 2016, Effect of the thermal treatment on the magnetic and structural properties of cobalt ferrite particles, *Ceram. Int.*, 42 (14), 15183–15188.

[10] Mmelesi, O.K., Masunga, N., Kuvarega, A., Nkambule, T.T.I., Mamba, B.B., and Kefeni, K.K., 2021, Cobalt ferrite nanoparticles and nanocomposites: Photocatalytic, antimicrobial activity and toxicity in water treatment, *Mater. Sci. Semicond. Process.*, 123, 105523.

[11] Baláž, P., Boldižárová, E., Godočíková, E., and Briančin, J., 2003, Mechanochemical route for sulphide nanoparticles preparation, *Mater. Lett.*, 57 (9-10), 1585–1589.

[12] Elsayed, M.R.A., Elseman, A.M., Abdelmageed, A.A., Hashem, H.M., and Hassen, A., 2023, Green and cost-effective morter grinding synthesis of bismuth-doped halide perovskites as efficient absorber materials, *J. Mater. Sci.: Mater. Electron.*, 34 (3), 194.

[13] Zeynizadeh, B., Gholamiyan, E., and Gilanizadeh, M., 2018, Magnetically recoverable $CuFe_2O_4$ nanoparticles as an efficient heterogeneous catalyst for green formylation of alcohols, *Curr. Chem. Lett.*, 7 (4), 121–130.

[14] Akbari Moayyer, H., and Ataie, A., 2014, Investigation on phase evolution in the processing of nano-crystalline cobalt ferrite by solid-state reaction route, *Adv. Mater. Res.*, 829, 767–771.

[15] Le, H.V., Nguyen, V.B., Pham, H.H., Nguyen, K.D., Ho, P.H., Trens, P., and Di Renzo, F., 2021, Combustion-synthesized porous CuO-CeO_2-SiO_2 composites as solid catalysts for the alkenylation of $C(sp^3)$-H bonds adjacent to a heteroatom via cross-dehydrogenative coupling, *Catalysts*, 11 (10), 1252.

[16] Ben-Arfa, B.A.E., Palamá, I.E., Miranda Salvado, I.M., Ferreira, J.M.F., and Pullar, R.C., 2020, The role of calcium (source & content) on the *in vitro* behaviour of sol–gel quaternary glass series, *Ceram. Int.*, 46 (1), 1065–1075.

[17] Cochran, E.A., Woods, K.N., Johnson, D.W., Page, C.J., and Boettcher, S.W., 2019, Unique chemistries of metal-nitrate precursors to form metal-oxide thin films from solution: Materials for electronic

and energy applications, *J. Mater. Chem. A*, 7 (42), 24124–24149.

[18] Yang, H., Zhang, X., Tang, A., and Qiu, G., 2004, Cobalt ferrite nanoparticles prepared by coprecipitation/mechanochemical treatment, *Chem. Lett.*, 33 (7), 826–827.

[19] Sivagurunathan, P., and Gibin, S.R., 2016, Preparation and characterization of nanosized cobalt ferrite particles by co-precipitation method with citrate as chelating agent, *J. Mater. Sci.: Mater. Electron.*, 27 (9), 8891–8898.

[20] Kalam, A., Al-Sehemi, A.G., Assiri, M., Du, G., Ahmad, T., Ahmad, I., and Pannipara, M., 2018, Modified solvothermal synthesis of cobalt ferrite ($CoFe_2O_4$) magnetic nanoparticles photocatalysts for degradation of methylene blue with H_2O_2/visible light, *Results Phys.*, 8, 1046–1053.

[21] Yu, M., Feng, Z., Huang, Y., Wang, K., and Liu, L., 2019, $CoFe_2O_4$ nanoparticles directly grown on carbon nanotube with coralline structure as anodes for lithium ion battery, *J. Mater. Sci.: Mater. Electron.*, 30 (4), 4174–4183.

[22] Qayoom, M., Shah, K.A., Pandit, A.H., Firdous, A., and Dar, G.N., 2020, Dielectric and electrical studies on iron oxide (α-Fe_2O_3) nanoparticles synthesized by modified solution combustion reaction for microwave applications, *J. Electroceram.*, 45 (1), 7–14.

[23] Kale, S.B., Somvanshi, S.B., Sarnaik, M.N., More, S.D., Shukla, S.J., and Jadhav, K.M., 2018, Enhancement in surface area and magnetization of $CoFe_2O_4$ nanoparticles for targeted drug delivery application, *AIP Conf. Proc.*, 1953 (1), 030193.

[24] Ortiz-Quiñonez, J.L., Pal, U., and Villanueva, M.S., 2018, Structural, magnetic, and catalytic evaluation of spinel Co, Ni, and Co–Ni ferrite nanoparticles fabricated by low-temperature solution combustion process, *ACS Omega*, 3 (11), 14986–15001.

[25] Reddy, M.P., Mohamed, A.M.A., Zhou, X.B., Du, S., and Huang, Q., 2015, A facile hydrothermal synthesis, characterization and magnetic properties of mesoporous $CoFe_2O_4$ nanospheres, *J. Magn. Magn. Mater.*, 388, 40–44.

[26] Cedeño-Mattei, Y., Perales-Pérez, O., and Uwakweh, O.N.C., 2013, Effect of high-energy ball milling time on structural and magnetic properties of nanocrystalline cobalt ferrite powders, *J. Magn. Magn. Mater.*, 341, 17–24.

[27] Ali, R.F., and Gates, B.D., 2018, Synthesis of lithium niobate nanocrystals with size focusing through an Ostwald ripening process, *Chem. Mater.*, 30 (6), 2028–2035.

[28] Sivakumar, M., Kanagesan, S., Umapathy, V., Suresh Babu, R., and Nithiyanantham, S., 2012, Study of $CoFe_2O_4$ particles synthesized with various concentrations of PVP polymer, *J. Supercond. Novel Magn.*, 26 (3), 725–731.

[29] Vadivel, M., Babu, R.R., Ramamurthi, K., and Arivanandhan, M., 2017, Effect of PVP concentrations on the structural, morphological, dielectric and magnetic properties of $CoFe_2O_4$ magnetic nanoparticles, *Nano-Struct. Nano-Objects*, 11, 112–123.

[30] Sui, Y., Huang, X., Ma, Z., Li, W., Qiao, F., Chen, K., and Chen, K., 2003, The effect of thermal annealing on crystallization in a-Si:H/SiO_2 multilayers by using layer by layer plasma oxidation, *J. Phys.: Condens. Matter*, 15 (34), 5793–5799.